ACS NANO
Cite This: ACS Nano 2019, 13, 9638–9646
www.acsnano.org

ARTICLE

Intrinsic Optoelectronic Characteristics of MoS_2 Phototransistors *via* a Fully Transparent van der Waals Heterostructure

Jinsu Pak,[†] Ilmin Lee,[‡] Kyungjune Cho,[†] Jae-Keun Kim,[†] Hyunhak Jeong,[†] Wang-Taek Hwang,[†] Geun Ho Ahn,[#] Keehoon Kang,[†] Woo Jong Yu,[‡,§] Ali Javey,[#] Seungjun Chung,*[,⊥] and Takhee Lee*[,†]

[†]Department of Physics and Astronomy, and Institute of Applied Physics, Seoul National University, Seoul 08826, Korea
[‡]Department of Electrical and Computer Engineering, Sungkyunkwan University, Suwon 16419, Korea
[#]Electrical Engineering and Computer Sciences, University of California, Berkeley, California 94720, United States
[§]Center for Integrated Nanostructure Physics, Institute for Basic Science (IBS), Suwon 16419, Republic of Korea
[⊥]Photo-Electronic Hybrids Research Center, Korea Institute of Science and Technology (KIST), Seoul 02792, Korea

S *Supporting Information*

ABSTRACT: **In the past decade, intensive studies on monolayer MoS_2-based phototransistors have been carried out to achieve further enhanced optoelectronic characteristics. However, the intrinsic optoelectronic characteristics of monolayer MoS_2 have still not been explored until now because of unintended interferences, such as multiple reflections of incident light originating from commonly used opaque substrates. This leads to overestimated photoresponsive characteristics inevitably due to the enhanced photogating and photoconductive effects. Here, we reveal the intrinsic photoresponsive characteristics of monolayer MoS_2, including its internal responsivity and quantum efficiency, in fully transparent monolayer MoS_2 phototransistors employing a van der Waals heterostructure. Interestingly, as opposed to the previous reports, the internal photoresponsive characteristics do not significantly depend on the wavelength of the incident light as long as the electron−hole pairs are generated in the same *k*-space. This study provides a deeper understanding of the photoresponsive characteristics of MoS_2 and lays the foundation for two-dimensional materials-based transparent phototransistors.**

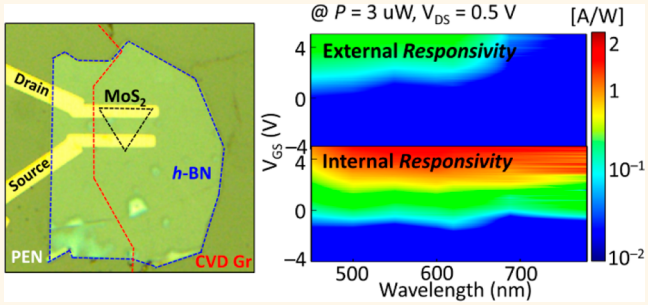

KEYWORDS: *MoS_2, phototransistor, heterostructure, internal quantum efficiency, internal responsivity*

Beginning with extensive research on graphene, the emergence of atomically thin two-dimensional (2D) materials has attracted substantial attention in the fundamental scientific studies and the next generation of electronics.[1−4] In this group of 2D materials, especially molybdenum disulfide (MoS_2) has been extensively studied as a promising candidate for realizing 2D materials-based flexible photodetectors due to its outstanding optoelectronic properties, such as intrinsic bandgap, high photodetection capability, high carrier mobility, good electrical stability, and mechanical flexibility.[5−10] Recently, MoS_2-based 2D heterostructures have been designed to enhance photodetection and photoswitching abilities, which is attributed to the high-quality interfacial properties between 2D materials held together by the weak van der Waals (vdW) interaction without covalent bonds. For instance, vdW heterostructured MoS_2 photodiodes made with tungsten diselenide (WSe_2), molybdenum ditelluride ($MoTe_2$), and black phosphorus have been realized to improve photoresponsive characteristics.[11−15] Also, MoS_2 phototransistors with hexagonal boron nitride (*h*-BN), graphene, and tin diselenide ($SnSe_2$) in a vertical vdW heterostructure have shown enhanced responsivity or faster photoswitching behaviors.[16−18] Although numerous results of the optoelectronic properties of vdW heterostructured photodetectors have been reported, to date, the intrinsic optoelectronic characteristics of atomically thin MoS_2 have not been explored because most previous studies have employed opaque substrates, typically heavily doped Si with

Received: June 19, 2019
Accepted: July 25, 2019
Published: July 25, 2019

DOI: 10.1021/acsnano.9b04829
ACS Nano 2019, 13, 9638–9646

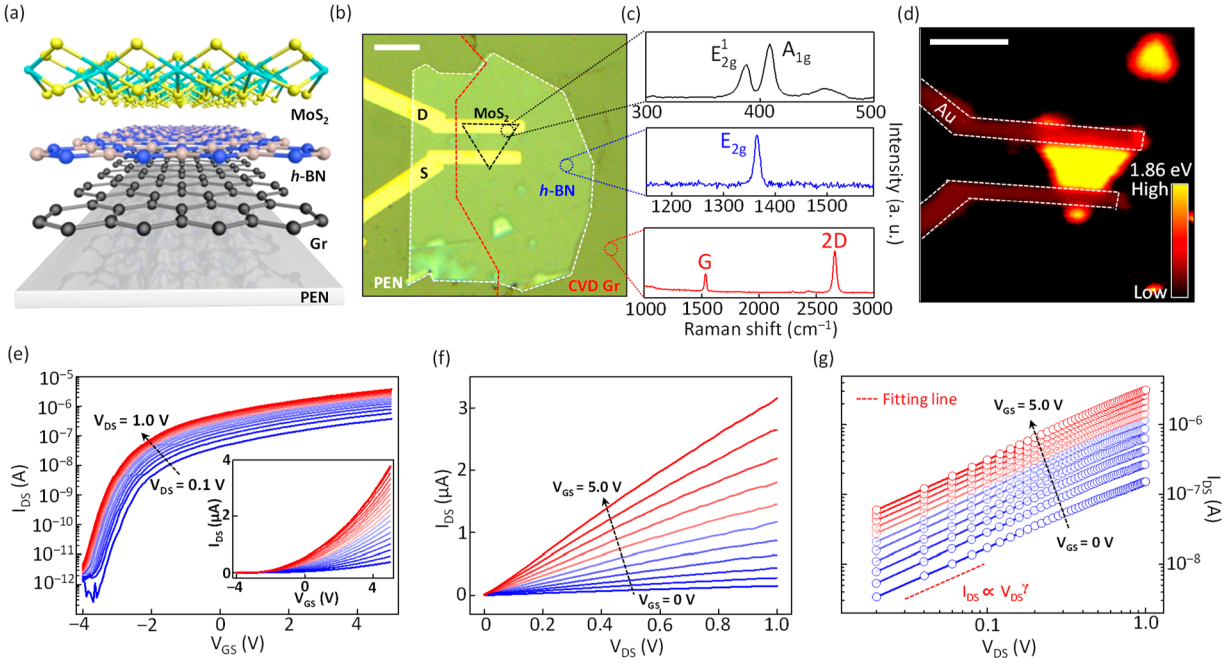

Figure 1. (a) Schematic of the vdW heterostructure on a PEN substrate. (b) Optical image of a fabricated fully transparent MoS_2 phototransistor. (c) Raman spectra for the CVD-grown monolayer MoS_2 and graphene (denoted as Gr) and mechanically exfoliated multilayer *h*-BN. Scale bar = 5 μm. (d) PL mapping image with a 1.86 eV peak intensity. Scale bar = 5 μm. (e) I_{DS}–V_{GS} and (f) I_{DS}–V_{DS} curves for the fully transparent MoS_2 phototransistor. (g) Logarithmic scale plot for I_{DS}–V_{DS} with an average γ value of 1.01.

SiO_2, due to the convenience from a manufacturing perspective. The opaque platforms allow multiple reflections of incident light, which results in the generation of additional electron–hole pairs at the MoS_2/SiO_2 and SiO_2/Si interfaces.[19] Furthermore, this unintended interference causes a strong photogating effect due to the trapping of photogenerated holes at the low-quality interface,[20,21] which can overestimate the ability of the photoresponsivity of MoS_2. For a better understanding of MoS_2, in this regard, the systematic investigation of the intrinsic optoelectronic characteristics of monolayer MoS_2 is highly desirable without effects caused by external interference such as reflected or refractive light.

Here, we report the intrinsic optoelectronic characteristics of monolayer MoS_2 phototransistors *via* a fully transparent vdW heterostructure with *h*-BN (as a dielectric layer) and graphene (as a gate electrode). The 2D *h*-BN dielectric provided a near-ideal interface with MoS_2 enabling low-voltage operation. To investigate the intrinsic photoresponsive properties of MoS_2, we compared the characteristics of the MoS_2 phototransistors fabricated on transparent polyethylene naphthalate (PEN) and opaque SiO_2/Si substrates. From the results, it turned out that the MoS_2 phototransistors fabricated on the opaque SiO_2/Si substrate showed higher photoresponsive performances due to the enhanced photogating and photoconductive effects caused by multiple reflections of the incident light. From the MoS_2 phototransistors fabricated on the transparent PEN substrate, the intrinsic photoresponsive properties were revealed; specifically, an internal responsivity of 3.2×10^2 A/W and internal quantum efficiency (IQE) of 7.1×10^5 % were achieved. Interestingly, unlike the external photoresponse determined by the incident photons that shows wavelength-dependent characteristics, the internal photoresponse determined by absorbed photons in the MoS_2 channel did not significantly depend on the wavelength of the incident light. Furthermore, we found that the intrinsic photoresponsive characteristics of MoS_2 could be dependent on the locations where photogeneration occurred in *k*-space and the consequent alteration of the effective mass.

RESULTS AND DISCUSSION

For the realization of transparent MoS_2 phototransistors, ready-made MoS_2 field-effect transistors (FETs) on a SiO_2/Si substrate were transferred to a PEN substrate *via* the transfer method using potassium hydroxide etching solution (see Methods and Figure S1 in the Supporting Information for more details of the fabrication process). To enhance the reproducibility of MoS_2 phototransistors, chemical vapor deposition (CVD)-grown monolayer MoS_2 was used as a channel layer in 2D vdW heterostructured FETs. In addition, by employing CVD-grown monolayer graphene as a gate electrode and mechanically exfoliated multilayer *h*-BN (41 nm thick) as a gate dielectric on a transparent PEN substrate (125 μm thick), good transparency of over 80% in the visible range was achieved. Figure 1a shows a schematic illustrating the vertically stacked vdW heterostructure on a PEN substrate. After the realization of the 2D heterostructure using a micromanipulator system (AP-4200GP, UNITEK), no drastically degraded transparency was observed in the optical image (Figure 1b). The Raman frequency difference (20 cm^{-1}) (upper panel, Figure 1c) and a photoluminescence (PL) mapping image displaying uniform bandgap energy (1.86 eV) (Figure 1d) support the fact that the CVD-grown MoS_2 used for the channel was a uniform monolayer.[22] In addition, the Raman peak observed for the multilayer *h*-BN at 1364 cm^{-1} is assigned to the in-plane vibration (E_{2g} mode).[23] The large intensity of the 2D-band relative to the G-band, which can only be observed in monolayer graphene due to a triple-resonance process, shows that monolayer graphene film was well grown *via* the optimized CVD process (lower panel, Figure 1c).[24] All

DOI: 10.1021/acsnano.9b04829
ACS Nano 2019, 13, 9638–9646

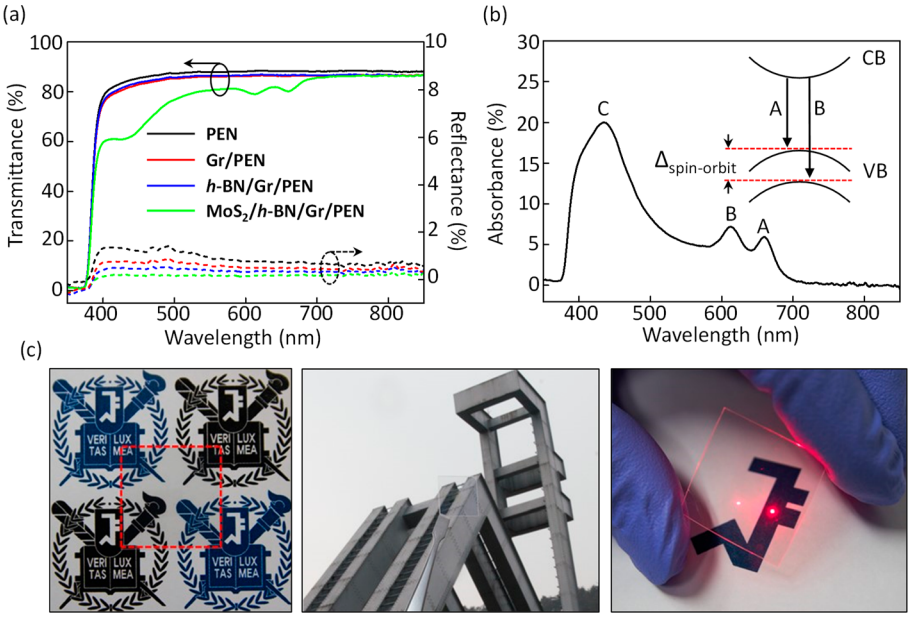

Figure 2. (a) Transmittances (solid lines) and reflectances (dashed lines) corresponding to each heterostructure. (b) Absorbance of the CVD-grown monolayer MoS_2 indicating three resonance peaks: A, B, and C. (c) Photographic images displaying high transparency.

Raman spectra in Figure 1c were measured before transfer to a PEN substrate for observing the distinct spectrum.

Figure 1e and f show the transfer curve (drain−source current *versus* gate voltage, I_{DS}−V_{GS}) and the output curve (drain−source current *versus* drain voltage, I_{DS}−V_{DS}) for the transparent CVD-grown monolayer MoS_2 FET measured under vacuum (~10^{-4} Torr) at room temperature. Arising from the thin *h*-BN dielectric layer, a low operation voltage ranging from −4 to 5 V was achieved. The maximum field-effect mobility (μ) was determined to be 12.2 $cm^2/V{\cdot}s$ (extracted at V_{GS} = 5 V and V_{DS} = 0.25 V), as calculated using the formula

$$\mu = \left(\frac{\partial I_{DS}}{\partial V_{GS}}\right)\frac{L}{WC_i}\frac{1}{V_{DS}} \quad (1)$$

with a channel width W = 8.56 μm, channel length L = 5.05 μm, and unit capacitance for the *h*-BN dielectric C_i = 0.756 mF/cm^2 (thickness of 41 nm and dielectric constant of 3.5 for *h*-BN were considered[25,26]). V_{GS}-dependent mobilities[27] at different V_{DS} are indicated in Figure S2 in the Supporting Information. Figure 1g shows the logarithmic scale plot for I_{DS}−V_{DS} measured at V_{GS} ranging from 0 to 5 V. The extracted average γ (linearity parameter in the output curve) value of 1.01 in the output characteristics indicates ohmic contacts between the MoS_2 channel layer and Au electrodes.

Figure 2a shows the transmittance and reflectance of the device on stacking the individual layers: transparent substrate (PEN), CVD-grown monolayer graphene (denoted as Gr)/PEN, *h*-BN/Gr/PEN, and CVD-grown monolayer MoS_2/*h*-BN/Gr/PEN. Negligible absorption in the visible range for Gr and multilayer *h*-BN was verified through the observation of unchanged transmittance values after stacking the Gr and *h*-BN layers onto a PEN substrate. The absorbance of CVD-grown monolayer MoS_2 was determined by subtracting the reflectance of the MoS_2 layer from the diminished transmittance after stacking the MoS_2 layer onto an underlying *h*-BN/Gr/PEN layer (Figure 2b). The extracted absorbance of the MoS_2 layer was used as a reference to investigate the internal optoelectronic characteristics by absorbed photons, not incident photons in the MoS_2 channel. In Figure 2b, the resonance peaks A and B correspond to excitonic transitions split by spin−orbit coupling at the K point in *k*-space.[22,28] The strong resonance peak C is ascribed to the parallel bands in the density of states even for excitation energy far exceeding the bandgap of MoS_2; this is called the band-nesting effect, which leads to a divergence in the joint density of states.[29,30] By employing transparent layers of Gr, MoS_2, *h*-BN, and PEN, fully transparent MoS_2 phototransistors were implemented with high transparency, as shown in Figure 2c. Also, the incident laser light fully penetrated through the fully stacked MoS_2 phototransistors without reflection or dispersion (right, Figure 2c).

To investigate the effects of the unintended photoresponsive characteristics, which are attributed to the use of an opaque substrate, CVD-grown monolayer MoS_2 phototransistors were fabricated with a *h*-BN dielectric on both a transparent PEN substrate (MoS_2/*h*-BN/Gr, denoted as MhG) and an opaque 100 nm thick SiO_2/Si substrate (MoS_2/*h*-BN/heavily doped silicon, denoted as MhS), as depicted in Figure 3a and b, respectively. The photoresponsive characteristics for MhG and MhS were investigated under various illumination conditions with different light intensities ranging from 15 to 1180 nW at a fixed wavelength of 450 nm and with different wavelengths ranging from 780 to 450 nm at a fixed light intensity of 3 μW in ambient air at room temperature (Figure 3c−f). Note that the diameter of the laser spot was ~1 μm, smaller than the channel area dimension, so that the entire laser light was focused within the MoS_2 channel area. As shown in Figure 3c−f, the photoinduced current steadily increased in both types of devices, MhG and MhS, as the illumination intensity became stronger at a fixed wavelength (Figure 3c and e) and also as the wavelength of the incident light became shorter at a fixed illumination intensity (Figure 3d and f). As shown in Figure 3d and f, the electron−hole pairs could be created by illumination with laser photon energy (1.59 and 1.80 eV, corresponding to 780 and 688 nm, respectively) smaller than the optical

DOI: 10.1021/acsnano.9b04829
ACS Nano 2019, 13, 9638−9646

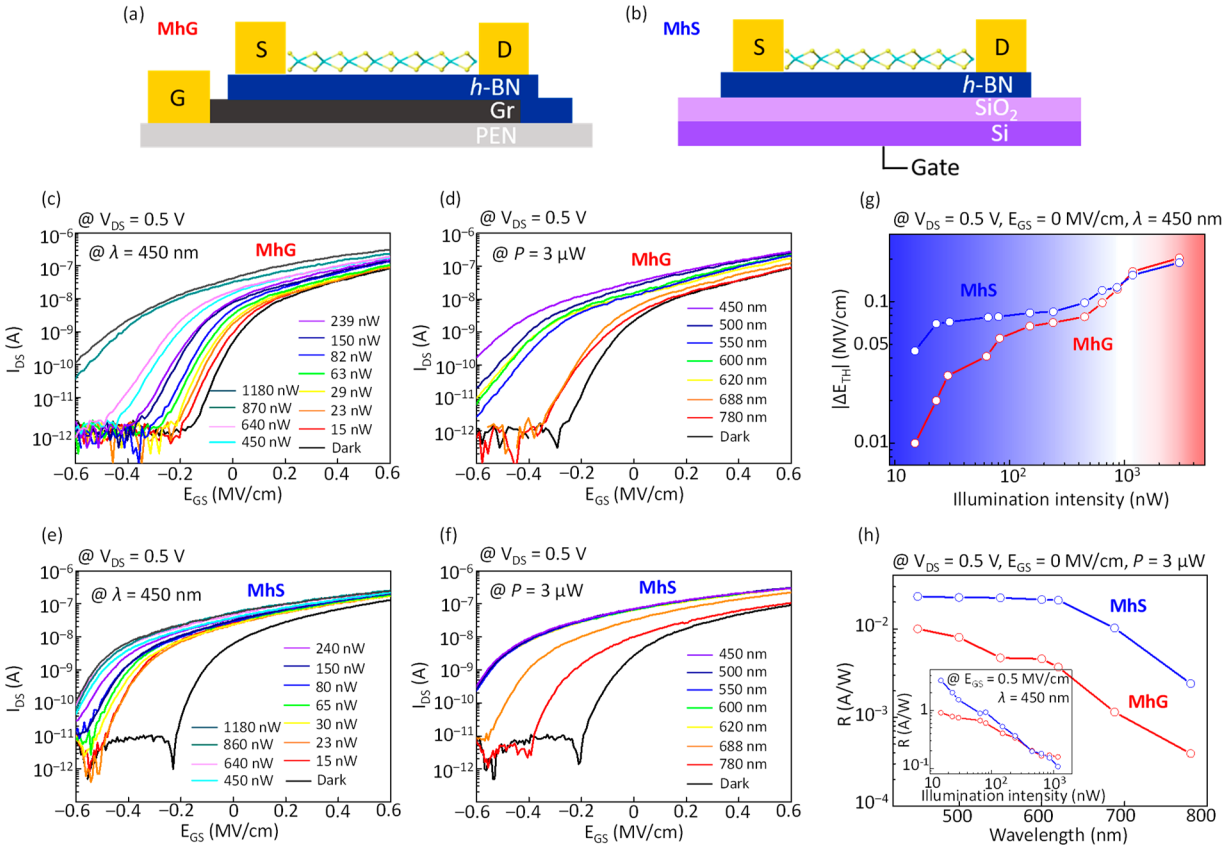

Figure 3. Schematics for (a) MhG and (b) MhS. The thickness for the multilayer *h*-BN was 41 and 28 nm for MhG and MhS, respectively. The range of E_{GS} (0.6 MV/cm) corresponds to an applied V_{GS} of 2.46 and 7.68 V for MhG and MhS, respectively. (c–f) Photoresponsive characteristics of MhG and MhS under various illumination conditions with light intensity ranging from 15 to 1180 nW at a fixed wavelength of 450 nm and wavelength ranging from 780 to 450 nm at a fixed intensity of 3 μW. (g) E_{TH} variation *versus* illumination intensity and (h) wavelength-dependent responsivity of MhG and MhS at a fixed V_{DS} of 0.5 V and E_{GS} of 0 MV/cm. The inset figure indicates the responsivity as a function of illumination intensity at a fixed E_{GS} of 0.5 MV/cm.

bandgap energy of MoS_2 (1.9 eV)[31] *via* the excitation of carriers localized in band tail states. For a more accurate comparison, the gate electric field (E_{GS}) instead of V_{GS} was used as the *x*-axis in Figure 3c–f because of the different thicknesses of the dielectric layers in MhG and MhS. Note that the contour plots visualizing the photoresponsive characteristics of MhG and MhS are indicated in Figure S4 in the Supporting Information. There were two noticeable distinctions in the photoresponsive characteristics for MhG and MhS: (1) the amount of change in the threshold electric field (ΔE_{TH}) in MhS due to illumination was larger than that in MhG (Figure 3g), and (2) the responsivity (R) of MhS was higher than that of MhG (Figure 3h). To understand the difference in the photoresponsive properties between MhG and MhS, the components of the photoinduced current should be classified.

To date, various mechanisms for the photoinduced current in MoS_2 have been proposed, such as the photoelectric (PE), photothermoelectric (PTE), photogating (PG), and photoconductive (PC) effects. Typically, the PE and PTE effects dominate in the photoresponse in cases without an electric field; therefore, the PG and PC effects dominantly determine the photoconductivity in phototransistors when an electric field is applied.[20] The PG effect is attributed to structural defects in MoS_2 itself or to disorder caused by the imperfect interface between MoS_2 and substrate at which the photogenerated electrons or holes can be trapped, playing the role of a local gate electric field. In addition, trapped charges in the dielectric layer itself can also contribute to the photogating effect. In n-type MoS_2-based FETs, a negative shift in the threshold voltage (V_{TH}) is typically observed due to the PG effect *via* the trapped photogenerated holes.[20] In contrast, the PC effect corresponds to the contribution of increased channel current due to the photogenerated carriers in the channel, which influence V_{TH} less. So, the total photocurrent (I_{Ph}) can be expressed as

$$I_{Ph} = I_{Ph,PG} + I_{Ph,PC} = g_m|\Delta V_{TH}| + \left(\frac{W}{L}\right)V_{DS}\Delta\sigma \quad (2)$$

where $g_m = \frac{dI_{DS}}{dV_{GS}}$ is the transconductance and $\Delta\sigma = q\mu_n\Delta n$ is the change in conductivity due to the photogenerated carriers. Although the proportion between the PG and PC effects differs depending on the device structure, typically, the PG effect is more dominant in vdW materials.[20] If photogenerated minority carriers are trapped with long lifetime depending on the nature of the trap state, they can produce an additional gate electric field until they disappear through recombination.[32,33] When the majority carriers pass through the channel for contributing to the photocurrent, additional majority carriers should be injected into the channel to preserve charge neutrality until the trapped photogenerated holes disappear.[32,33] Therefore, the photoresponsive characteristics in vdW materials-based phototransistors can be amplified by

DOI: 10.1021/acsnano.9b04829
ACS Nano 2019, 13, 9638–9646

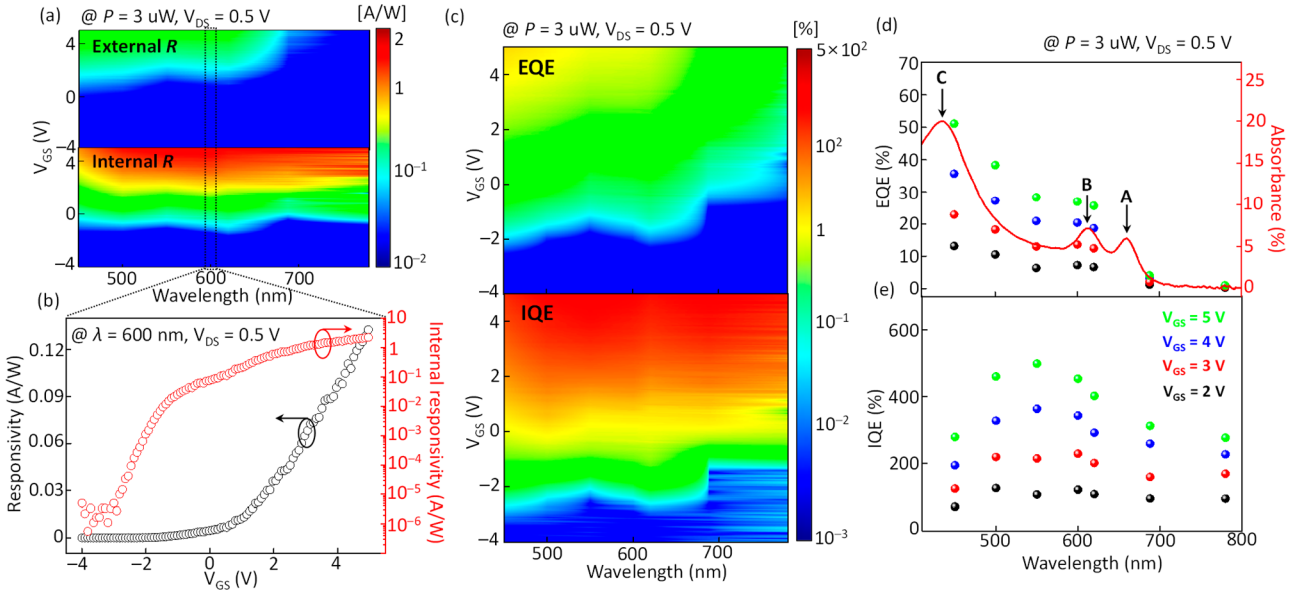

Figure 4. (a) Contour plots indicating external (upper panel) and internal (lower panel) responsivities as a function of V_{GS} and wavelength at a fixed V_{DS} of 0.5 V and illumination intensity of 3 μW. (b) External and internal responsivities at a fixed wavelength of 600 nm. (c) Contour plots comparing EQE (upper panel) and IQE (lower panel) at a fixed V_{DS} of 0.5 V and illumination intensity of 3 μW. The wavelength-dependent (d) EQE and (e) IQE values (colored circle symbols) corresponding to each V_{GS}. Absorbance for a CVD-grown MoS_2 monolayer is indicated as a red solid line in (d).

trapping photogenerated minority carriers as well as by applied electric fields for accelerating the movement of the majority carriers.

In this regard, the higher value of $|\Delta E_{TH}|$ for MhS in the low illumination intensity regime than that for MhG (blue area in Figure 3g) indicates that the PG effect in MhS was stronger than that in MhG in the low illumination intensity regime. This behavior is due to the influence of the reflected light from the SiO_2/Si substrate along with the PG effect. The reflectance spectra of the device fabricated on the SiO_2/Si substrate are provided in Figure S5 in the Supporting Information. In our study, the PG effect arises dominantly from the trapped holes at the intrinsic defects such as sulfur vacancies in MoS_2,[34] but not at the interface trap sites because the underlying inserted *h*-BN layer provided a near-ideal interface with MoS_2. Therefore, the reflected light from the SiO_2/Si substrate in MhS can generate more trapped photogenerated holes, which leads to the enhanced PG effect in MhS in the low illumination intensity regime. However, in the high illumination intensity regime, most trap sites can be occupied by sufficient photogenerated holes in both MhS and MhG. Thus, the values for $|\Delta E_{TH}|$ for MhS and MhG became comparable in the high illumination intensity regime (red area in Figure 3g).

Figure 3h shows the responsivity for MhS and MhG as a function of wavelength measured at a fixed V_{DS} of 0.5 V, E_{GS} of 0 MV/cm, and illumination intensity (P) of 3 μW. Note that the maximum power for the illumination intensity was restricted up to 3 μW to prevent any undesirable physical damage to the atomically thin monolayer MoS_2 channel. The responsivity (R) is an important parameter for evaluating the performance for photodetector applications, which is defined as

$$R = \frac{I_{Ph}}{P_{Inc}} \quad (3)$$

where P_{Inc} is the incident illumination intensity. We observed a higher responsivity for MhS than that for MhG under various wavelengths ranging from 780 to 450 nm at a fixed intensity of 3 μW, as shown in Figure 3h. This result is also attributed to the light reflected from the SiO_2/Si substrate along with the PC effect. Because the PG effects in MhS and MhG are comparable under high-intensity illumination, the reason for the higher responsivity of MhS is attributed to the stronger PC effect in MhS, which originates from additional carrier creation by the reflected light from the SiO_2/Si substrate (Figure 3h). It should be noted that the calculated number of densities-of-state at the interface MoS_2/*h*-BN are 3.41×10^{12} and 3.07×10^{12} cm^{-2} eV^{-1} for the MhS and MhG, respectively (see Section 6 in the Supporting Information).[35,36] This result supports that the different responsivities are the effect originated from the opaque substrate, not from the interfacial defects. In addition, the responsivity under the various illumination intensities ranging from 15 to 1180 nW at a fixed wavelength of 450 nm and E_{GS} of 0.5 MV/cm is indicated in the inset of Figure 3h. Due to the stronger PG effect in MhS in the low illumination intensity regime, a higher responsivity was observed in MhS than in MhG; then, the responsivity values became comparable between MhS and MhG as the illumination intensity was increased (inset of Figure 3h). As the illumination intensity increased, the responsivities for both MhS and MhG were reduced. Note that an opposite result, *i.e.*, enhanced responsivity with increasing intensity, can be observed at different E_{GS} (see Figure S6 in the Supporting Information). These different tendencies of the responsivity *versus* illumination intensity are primarily determined by the applied E_{GS} regardless of their different device structures, because the charge carrier dynamics can be changed by the locations of the Fermi level of MoS_2 set by the applied E_{GS} (see Figures S7 and S8 in the Supporting Information for details). The decline of the responsivity for increasing illumination intensity can be explained in terms of restricted trap sites. In

DOI: 10.1021/acsnano.9b04829
ACS Nano 2019, 13, 9638−9646

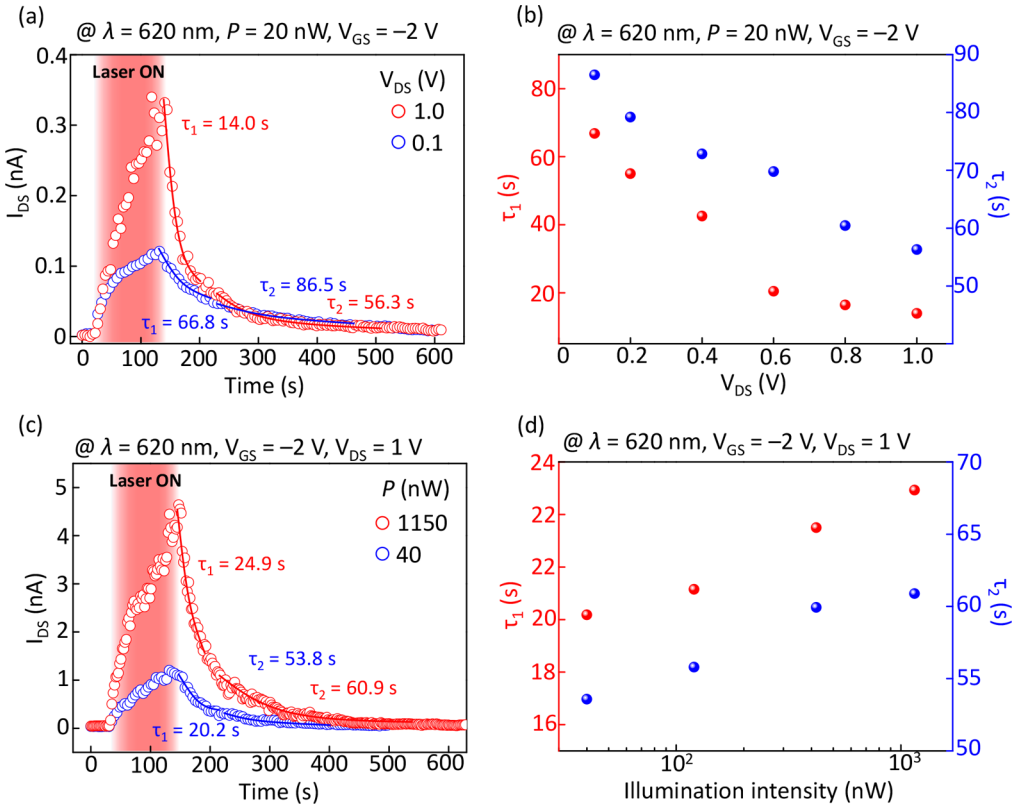

Figure 5. (a) Photoswitching characteristics of a fully transparent MoS_2 phototransistor under illumination of the MoS_2 channel for 100 s at different V_{DS} conditions of 1.0 V (red open circle symbols) and 0.1 V (blue open circle symbols) at a fixed V_{GS} of −2 V. The solid lines are lines fitted by an exponential decay function. (b) τ_1 and τ_2 *versus* V_{DS} ranging from 0.1 to 1.0 V. (c) Photoswitching characteristics at different illumination intensities of 1150 nW (red open circle symbols) and 40 nW (blue open circle symbols) at a fixed V_{DS} of 1 V. (d) τ_1 and τ_2 *versus* the illumination intensity ranging from 40 to 1150 nW.

the low illumination intensity regime, a substantial portion of the photogenerated holes can be trapped and act as a positive gate electric field, leading to increased responsivity. On the other hand, in the high illumination intensity regime, the possibility that the photogenerated holes can be trapped becomes lower due to the limited number of trap sites compared to the increased number of carriers. Therefore, the MoS_2 phototransistors exhibit a higher responsivity under the low illumination intensity.[37−39] In addition, the increased recombination rate originating from the high density of photogenerated carriers can also lead to the reduced responsivity. For these reasons, the MoS_2 phototransistors exhibit a lower responsivity under a high illumination intensity. Therefore, through a comparative analysis between MhG and MhS, it was observed that the photoresponsive characteristics of MoS_2 phototransistors fabricated on opaque substrates are overestimated, which cannot be regarded as the intrinsic optoelectronic characteristics of monolayer MoS_2.

To explore the intrinsic optoelectronic properties of MoS_2, the dependencies of the optoelectronic characteristics of transparent MhG on V_{GS} and wavelength were investigated (Figure 4). Note that the intrinsic optoelectronic results under the various illumination intensities are provided in Figures S7−S9 in the Supporting Information. The contour plots indicating external and internal responsivities as a function of V_{GS} and wavelength measured at a V_{DS} of 0.5 V are displayed in Figure 4a. Because the internal responsivity value is defined as the photocurrent per watt of the absorbed illumination intensity, the internal responsivity is calculated by dividing the external responsivity by the absorbance of the MoS_2 layer (Figure 2b) as follows:

$$\text{Internal responsivity} = \frac{I_{Ph}}{P_{Abs}} \tag{4}$$

where P_{Abs} is defined as absorbed illumination intensity ($P_{Inc} = P_{Abs} + P_{Tr} + P_{Ref}$, where P_{Tr} and P_{Ref} are transmitted and reflected illumination intensities, respectively). In other words, the values for the internal responsivity are higher than those for the external responsivity under the entire range of wavelengths (Figure 4a). To achieve the maximum responsivity in phototransistors, low illumination intensity, high V_{DS}, and high V_{GS} are required (for details, see Figure S7 in the Supporting Information). Under optimum measurement conditions, a maximum external responsivity of 16.8 A/W and maximum internal responsivity of 3.2×10^2 A/W were achieved (Figure S10 in the Supporting Information). Figure 4c exhibits contour plots comparing the external quantum efficiency (EQE) and internal quantum efficiency (IQE) *versus* V_{GS} and wavelength for a transparent MoS_2 phototransistor measured at a V_{DS} of 0.5 V and illumination intensity of 3 μW. EQE and IQE are defined as the number of carriers detected per incident photon and absorbed photon, respectively, as defined by the following formula:

$$\text{EQE}\ (\%) = \frac{I_{Ph/e}}{P_{Inc/h\nu}} \times 100 \text{ and IQE}\ (\%) = \frac{I_{Ph/e}}{P_{Abs/h\nu}} \times 100 \tag{5}$$

DOI: 10.1021/acsnano.9b04829
ACS Nano 2019, 13, 9638−9646

where e and $h\nu$ are elementary charge and photon energy, respectively. Similar to the dependency of the responsivity on V_{GS} (Figure 4b), EQE and IQE also increased with increasing V_{GS} at a fixed V_{DS} of 0.5 V (Figure 4c). For an in-depth understanding of the quantum efficiency dependence on the wavelength of the light, the EQE values extracted from the contour plot of Figure 4c are exhibited in Figure 4d. Note that the condition of $V_{GS} > V_{TH}$ ranging from 2 to 5 V was taken into account in Figure 4d and e, in which photogenerated carriers can contribute to the photocurrent efficiently. An abrupt increase in EQE was observed at a wavelength of around 620 nm due to the A- and B-excitonic transitions represented as the resonance peaks in the absorbance of MoS_2 (red line curve in Figure 4d). A higher EQE was also observed near the strong resonance peak at ~440 nm, corresponding to the C-excitonic transition induced by the band-nesting effect.[29,30]

In contrast, the IQE values by the C-excitonic transition were lower than those by the A- or B-excitonic transition, as shown in Figure 4e. Previous studies of the C-excitonic transition in MoS_2 reported that the photogenerated electrons and holes in the band-nesting region are well separated in k-space to their immediate band extremum.[30,40] Because the photogenerated electrons and holes in the band-nesting region move quickly to the Λ valley and Γ hill,[29,30,40] respectively, on an extremely fast intraband relaxation time scale of C-exciton (<500 fs),[41] a more enhanced photodetection ability could be expected under the C-excitonic transition due to the suppression of direct band-to-band recombination.[39] However, contrary to this anticipation, the photogenerated carriers excited by the A- or B-excitonic transition produced a higher IQE than that produced by the C-excitonic transition (Figure 4e). Note that a similar consequence was observed in the internal responsivity (see Figure S11 in the Supporting Information). These phenomena can be explained by the different effective masses of the carriers located at different positions in k-space. For the photodetection ability in n-type MoS_2 phototransistors, the effective mass of the electron is typically a more significant parameter because majority carriers (electrons) are accelerated by applied electric fields, thus contributing to the photocurrent, while minority carriers (holes) are trapped with a long lifetime. However, regardless of the types of carriers, the effective mass of the electron (hole) located at the Λ valley (Γ hill) created by the C-excitonic transition is heavier than that created by the A- or B-excitonic transitions at the K point.[42,43] In this manner, although the electron−hole pairs photogenerated by the C-excitonic transition can be easily separated without extinction by recombination, the IQE values under illumination at 450 nm (C-excitonic transitions) were 58% of those under illumination at 600 nm (B-excitonic transition), as extracted from the results measured at a V_{GS} from 2 to 5 V (Figure 4e). Interestingly, in contrast to the EQE and external responsivity, the IQE and internal responsivity did not exhibit a significant dependence on the wavelength of visible light. In addition, the IQE can also be amplified up to 7.1×10^5 % by the applied electric fields (V_{GS} and V_{DS}) under low illumination intensity (Figure S10 in the Supporting Information).

We investigated the temporal evolution of the photoresponse of MhG measured at a V_{DS} of 1.0 and 0.1 V and at a fixed V_{GS} of −2 V (illuminated by a laser with a wavelength of 620 nm and an intensity of 20 nW), as shown in Figure 5a. After illuminating the MoS_2 channel for 100 s, the decay process for the photoinduced current was examined after turning the laser off. Note that we intentionally limited the illumination time to 100 s because prolonged illumination can cause a persistent photoconductivity (PPC) effect, which shows a sustained conductivity even after the light is turned off. The PPC phenomenon is one of the critical unintended effects to achieve reliable optoelectronic characteristics of MoS_2 under repeatedly conducted experiments (see Figure S12 in the Supporting Information). The decay process followed an exponential decay function with two different decay constants (τ_1 and τ_2) according to the time range.[44] Even though high-quality MoS_2 phototransistors with a vdW heterostructure were realized, a long-lasting photoconductivity was inevitably observed after turning the laser off (Figure 5).[16,20,37] The origin for the long-lasting photoconductivity in the decay has been described as being due to the influence of random local potential fluctuations (RLPF) in the band structure[45,46] and the influence of the trapped photogenerated minority carriers that hinder recombination in the forbidden gap of MoS_2.[16,32−34] The confined carriers can escape the potential even after the laser is turned off and then contribute to the photocurrent, resulting in a long decay time. In addition, the trapped photogenerated holes in MoS_2 consistently induce the injection of electrons for charge neutrality until they disappear through the recombination process. In this regard, the increase in V_{DS} from 0.1 to 1.0 V promoted the release of confined carriers in RLPF and reduced the lifetime of the trapped photogenerated holes, so the τ_1 (τ_2) value decreased from 66.8 s (86.5 s) to 14.0 s (56.3 s), as shown in Figure 5a and b. Figure 5c shows the time-resolved photoresponse under illumination with different intensities of 1150 and 40 nW measured at a fixed V_{GS} of −2 V and V_{DS} of 1 V (illuminated by a laser with a wavelength of 620 nm). Because the high illumination intensity created more photogenerated electron−hole pairs, which leads to increased carrier confinement in RLPF or in the trap sites in the forbidden gap, the τ_1 (τ_2) value increased from 20.2 s (53.8 s) to 24.9 s (60.9 s) as the illumination intensity was increased from 40 nW to 1150 nW (Figure 5d). Also, the time-resolved photoresponse was not significantly affected by the wavelength of the laser because different photon energies cannot change the lifetime of the photogenerated holes trapped in the forbidden gap of MoS_2 (Figure S13 in the Supporting Information).

CONCLUSIONS

This work explores the internal optoelectronic characteristics of monolayer MoS_2 in fully transparent phototransistors by employing a 2D vdW heterostructure. From the systematic comparison of the optoelectronic characteristics between transparent and opaque MoS_2 phototransistors, it turns out that the photoresponsive characteristics of MoS_2 are overestimated due to enhanced photogating and photoconductive effects originating from the use of opaque substrates. In addition, we found that a maximum internal responsivity of 3.2×10^2 A/W and IQE of 7.1×10^5 % were yielded in a fully transparent MoS_2 phototransistor, which can be regarded as the intrinsic optoelectronic characteristics of CVD-grown monolayer MoS_2. Interestingly, in contrast with the external photoresponse, which was highly wavelength-dependent, the internal photoresponse did not significantly depend on the wavelength of the incident light. Furthermore, relatively lower IQE values at the C-excitonic transitions than those at the A- or B-excitonic transition show different optoelectronic proper-

DOI: 10.1021/acsnano.9b04829
ACS Nano 2019, 13, 9638−9646

ties depending on the locations of the photogenerated carriers in *k*-space due to their different effective masses. Our study will shed light on the understanding of the intrinsic optoelectronic characteristics of CVD-grown monolayer MoS_2, and it will provide deep insight into the realization of 2D materials-based transparent optoelectronics.

METHODS

Fabrication of Fully Transparent MoS_2 FETs. To fabricate fully transparent MoS_2 FETs, large-area monolayer graphene grown on a copper foil by the CVD method was transferred onto a 270 nm thick SiO_2/Si substrate. Next, a mechanically exfoliated multilayer *h*-BN was transferred onto the monolayer graphene by a micromanipulator system (AP-4200GP, UNITEK). After transferring the CVD-grown monolayer MoS_2 onto the *h*-BN, the Au source and drain electrodes (30 nm thick) were formed through processes using electron beam lithography (JSM-6510, JEOL) and an electron beam evaporator (KVE-2004L, Korea Vacuum Tech.). For transfer onto a transparent substrate, the vdW heterostructured MoS_2 FETs coated with poly(methyl methacrylate) (PMMA) were immersed into a 50% potassium hydroxide solution with annealing at 70 °C to etch the SiO_2/Si substrate. After that, the vdW heterostructure with the source and drain electrodes, which was held firmly by PMMA, was scooped up and transferred onto a 125 μm thick PEN substrate. The fabricated transparent MoS_2 FETs were annealed at 80 °C in a vacuum for 2 h to eliminate residues on the surface of the MoS_2 channels.

Electrical and Optical Characterization. The electrical properties of the transparent MoS_2 FETs were measured using a semiconductor parameter analyzer (Keithley 4200-SCS) in a vacuum. Transmittance and reflectance data for the vdW heterostructure were obtained by using a UV/vis/NIR microspectrometer (CRAIC, QDI-1000). Raman spectra, PL spectra, and PL mapping of vdW materials were characterized using an XperRam 200 (Nanobase, Inc.) instrument using a 532 nm laser as the excitation source with a diffraction-limited laser spot size (~1 μm spot radius). In addition, an electroluminescence measurement system (Nanobase, Inc.) was used to investigate the optoelectronic characteristics of the transparent MoS_2 phototransistors.

ASSOCIATED CONTENT

Supporting Information

The Supporting Information is available free of charge on the ACS Publications website at DOI: 10.1021/acsnano.9b04829.

Details on the device fabrication of the fully transparent MoS_2 phototransistor, electrical characteristics of the opaque MoS_2 phototransistor, internal responsivity and internal detectivity of transparent MoS_2 phototransistor, the responsivity depending on illumination intensity, investigation of field-dependent and wavelength-dependent optoelectronic characteristics, and time-resolved photoresponsive characteristics depending on wavelength of incident light (PDF)

AUTHOR INFORMATION

Corresponding Authors

*E-mail: seungjun@kist.re.kr.
*E-mail: tlee@snu.ac.kr.

ORCID

Geun Ho Ahn: 0000-0002-4761-7804
Woo Jong Yu: 0000-0002-7399-307X
Takhee Lee: 0000-0001-5988-5219

Notes

The authors declare no competing financial interest.

ACKNOWLEDGMENTS

The authors appreciate the financial support from the National Creative Research Laboratory program (Grant No. 2012026372) through the National Research Foundation of Korea funded by the Korean Ministry of Science and ICT. S.C. appreciates the support of the National Research Foundation of Korea (NRF) grant funded by the Ministry of Science and ICT of Korea (NRF-2017R1C1B2002323). W.J.Y. acknowledge the Institute for Basic Science (IBS-R011-D1). G.H.A. and A.J. acknowledge the Electronic Materials Program, funded by the Director, Office of Science, Office of Basic Energy Sciences, Material Sciences and Engineering Division of the U.S. Department of Energy under Contract No. DE-AC02-05CH11231.

REFERENCES

(1) Wang, Q. H.; Kalantar-Zadeh, K.; Kis, A.; Coleman, J. N.; Strano, M. S. Electronics and Optoelectronics of Two-Dimensional Transition Metal Dichalcogenides. *Nat. Nanotechnol.* **2012**, *7*, 699–712.

(2) Manzeli, S.; Ovchinnikov, D.; Pasquier, D.; Yazyev, O. V.; Kis, A. 2D Transition Metal Dichalcogenides. *Nat. Rev. Mater.* **2017**, *2*, 17033.

(3) Mak, K. F.; Shan, J. Photonics and Optoelectronics of 2D Semiconductor Transition Metal Dichalcogenides. *Nat. Photonics* **2016**, *10*, 216–226.

(4) Bhimanapati, G. R.; Lin, Z.; Meunier, V.; Jung, Y.; Cha, J.; Das, S.; Xiao, D.; Son, Y.; Strano, M. S.; Cooper, V. R.; Liang, L.; Louie, S. G.; Ringe, E.; Zhou, W.; Kim, S. S.; Naik, R. R.; Sumpter, B. G.; Terrones, H.; Xia, F.; Wang, Y.; et al. Recent Advances in Two-Dimensional Materials Beyond Graphene. *ACS Nano* **2015**, *9*, 11509.

(5) Zhang, W.; Huang, J.-K.; Chen, C.-H.; Chang, Y.-H.; Cheng, Y.-J.; Li, L.-J. High-Gain Phototransistors Based on a CVD MoS_2 Monolayer. *Adv. Mater.* **2013**, *25*, 3456–3461.

(6) Yoon, Y.; Ganapathi, K.; Salahuddin, S. How Good Can Monolayer MoS_2 Transistors Be? *Nano Lett.* **2011**, *11*, 3768–3773.

(7) Yoo, G.; Hong, S.; Heo, J.; Kim, S. Enhanced Photoresponsivity of Multilayer MoS_2 Transistors Using High Work Function MoO_X Overlayer. *Appl. Phys. Lett.* **2017**, *110*, 053112.

(8) Yang, S.; Park, S.; Jang, S.; Kim, H.; Kwon, J.-Y. Electrical Stability of Multilayer MoS_2 Field-Effect Transistor under Negative Bias Stress at Various Temperatures. *Phys. Status Solidi RRL* **2014**, *8*, 714–718.

(9) Chang, H.-Y.; Yang, S.; Lee, J.; Tao, L.; Hwang, W.-S.; Jena, D.; Lu, N.; Akinwande, D. High-Performance, Highly Bendable MoS_2 Transistors with High-K Dielectrics for Flexible Low-Power Systems. *ACS Nano* **2013**, *7*, 5446–5452.

(10) Seo, J.-W. T.; Zhu, J.; Sangwan, V. K.; Secor, E. B.; Wallace, S. G.; Hersam, M. C. Fully Inkjet-Printed, Mechanically Flexible MoS_2 Nanosheet Photodetectors. *ACS Appl. Mater. Interfaces* **2019**, *11*, 5675–5681.

(11) Furchi, M. M.; Pospischil, A.; Libisch, F.; Burgdörfer, J.; Mueller, T. Photovoltaic Effect in an Electrically Tunable van der Waals Heterojunction. *Nano Lett.* **2014**, *14*, 4785–4797.

(12) Lee, C.-H.; Lee, G.-H.; van der Zande, A. M.; Chen, W.; Li, Y.; Han, M.; Cui, X.; Arefe, G.; Nuckolls, C.; Heinz, T. F.; Guo, J.; Hone, J.; Kim, P. Atomically Thin *p-n* Junctions with van der Waals Heterointerfaces. *Nat. Nanotechnol.* **2014**, *9*, 676–681.

(13) Wang, F.; Yin, L.; Wang, Z. X.; Xu, K.; Wang, F. M.; Shifa, T. A.; Huang, Y.; Jiang, C.; He, J. Configuration-Dependent Electrically Tunable van der Waals Heterostructures Based on $MoTe_2/MoS_2$. *Adv. Funct. Mater.* **2016**, *26*, 5499–5506.

(14) Pezeshki, A.; Shokouh, S. H. H.; Nazari, T.; Oh, K.; Im, S. Electric and Photovoltaic Behavior of a Few-Layer α-$MoTe_2/MoS_2$ Dichalcogenide Heterojuction. *Adv. Mater.* **2016**, *28*, 3216–3222.

DOI: 10.1021/acsnano.9b04829
ACS Nano 2019, 13, 9638–9646

(15) Ye, L.; Li, H.; Chen, Z.; Xu, J. Near-Infrared Photodetector Based on MoS_2/black Phosphorus Heterojunction. *ACS Photonics* **2016**, *3*, 692−699.
(16) Tran, M. D.; Kim, J.-H.; Kim, H.; Doan, M. H.; Duong, D. L.; Lee, Y. H. Role of Hole Trap Sites in MoS_2 for Inconsistency in Optical and Electrical Phenomena. *ACS Appl. Mater. Interfaces* **2018**, *10*, 10580−10586.
(17) Zhang, W.; Chuu, C.-P.; Huang, J.-K.; Chen, C.-H.; Tsai, M.-L.; Chang, Y.-H.; Liang, C.-T.; Chen, Y.-Z.; Chueh, Y.-L.; He, J.-H.; Chou, M.-Y.; Li, L.-J. Ultrahigh-Gain Photodetectors Based on Atomically Thin Graphene-MoS_2 Heterostructures. *Sci. Rep.* **2015**, *4*, 3826.
(18) Zhou, X.; Zhou, N.; Li, C.; Song, H.; Zhang, Q.; Hu, X.; Gan, L.; Li, H.; Lü, J.; Luo, J.; Xiong, J.; Zhai, T. Vertical Heterostructures Based on $SnSe_2$/MoS_2 for High Performance Photodetectors. *2D Mater.* **2017**, *4*, 025048.
(19) Lien, D.-H.; Kang, J. S.; Amani, M.; Chen, K.; Tosun, M.; Wang, H.-P.; Roy, T.; Eggleston, M. S.; Wu, M. C.; Dubey, M.; Lee, S.-C.; He, J. H.; Javey, A. Engineering Light Outcoupling in 2D Materials. *Nano Lett.* **2015**, *15*, 1356−1361.
(20) Furchi, M. M.; Polyushkin, D. K.; Pospischil, A.; Mueller, T. Mechanisms of Photoconductivity in Atomically Thin MoS_2. *Nano Lett.* **2014**, *14*, 6165−6170.
(21) Huang, H.; Wang, J.; Hu, W.; Liao, L.; Wang, P.; Wang, X.; Gong, F.; Chen, Y.; Wu, G.; Luo, W.; Shen, H.; Lin, T.; Sun, J.; Meng, X.; Chen, X.; Chu, J. Highly Sensitive Visible to Infrared $MoTe_2$ Photodetectors Enhanced by the Photogating Effect. *Nanotechnology* **2016**, *27*, 445201.
(22) Splendiani, A.; Sun, L.; Zhang, Y.; Li, T.; Kim, J.; Chim, C.-Y.; Galli, G.; Wang, F. Emerging Photoluminescence in Monolayer MoS_2. *Nano Lett.* **2010**, *10*, 1271−1275.
(23) Song, L.; Ci, L.; Lu, H.; Sorokin, P. B.; Jin, C.; Ni, J.; Kvashnin, A. G.; Kvashnin, D. G.; Lou, J.; Yakobson, B. I.; Ajayan, P. M. Large Scale Growth and Characterization of Atomic Hexagonal Boron Nitride Layers. *Nano Lett.* **2010**, *10*, 3209−3215.
(24) Calizo, I.; Bejenari, I.; Rahman, M.; Liu, G.; Balandin, A. A. Ultraviolet Raman Microscopy of Single and Multilayer Graphene. *J. Appl. Phys.* **2009**, *106*, 043509.
(25) Dean, C. R.; Young, A. F.; Meric, I.; Lee, C.; Wang, L.; Sorgenfrei, S.; Watanabe, K.; Taniguchi, T.; Kim, P.; Shepard, K. L.; Hone, J. Boron Nitride Substrates for High-Quality Graphene Electronics. *Nat. Nanotechnol.* **2010**, *5*, 722−726.
(26) Kim, K. K.; Hsu, A.; Jia, X.; Kim, S. M.; Shi, Y.; Dresselhaus, M.; Palacios, T.; Kong, J. Synthesis and Characterization of Hexagonal Boron Nitride Film as a Dielectric Layer for Graphene Devices. *ACS Nano* **2012**, *6*, 8583−8590.
(27) Di Bartolomeo, A.; Genovese, L.; Giubileo, F.; Lemmo, L.; Luongo, G.; Foller, T.; Schleberger, M. Hysteresis in the Transfer Characteristics of MoS_2 Transistors. *2D Mater.* **2018**, *5*, 015014.
(28) Zhang, Y.; Li, H.; Wang, H.; Liu, R.; Zhang, S.-L.; Qiu, Z.-J. On Valance-Band Splitting in Layered MoS_2. *ACS Nano* **2015**, *9*, 8514−8519.
(29) Carvalho, A.; Ribeiro, R. M.; Neto, A. H. C. Band Nesting and the Optical Response of Two-Dimensional Semiconducting Transition Metal Dichalcogenides. *Phys. Rev. B: Condens. Matter Mater. Phys.* **2013**, *88*, 115205.
(30) Wang, L.; Wang, Z.; Wang, H.-Y.; Grinblat, G.; Huang, Y.-L.; Wang, D.; Ye, X.-H.; Li, X.-B.; Bao, Q.; Wee, A. T.-S.; Maier, S. A.; Caldwell, J. D.; Liberato, S. D. Slow Cooling and Efficient Extraction of C-exciton Hot Carriers in MoS_2 Monolayer. *Nat. Commun.* **2017**, *8*, 13906.
(31) Mak, K. F.; Lee, C.; Hone, J.; Shan, J.; Heinz, T. F. Atomically Thin MoS_2: A New Direct-Gap Semiconductor. *Phys. Rev. Lett.* **2010**, *105*, 136805.
(32) Buscema, M.; Island, J. O.; Groenendijk, D. J.; Blanter, S. I.; Steele, G. A.; van der Zant, H. S. J.; Castellanos-Gomez, A. Photocurrent Generation with Two-Dimensional van der Waals Semiconductors. *Chem. Soc. Rev.* **2015**, *44*, 3691−3718.
(33) Fang, H.; Hu, W. Photogating in Low Dimensional Photodetectors. *Adv. Sci.* **2017**, *4*, 1700323.
(34) Di Bartolomeo, A.; Genovese, L.; Foller, T.; Giubileo, F.; Luongo, G.; Croin, L.; Liang, S.-J.; Ang, L. K.; Schleberger, M. Electrical Transport and Persistent Photoconductivity in Monolayer MoS_2 Phototransistors. *Nanotechnology* **2017**, *28*, 214002.
(35) Kim, T.-Y.; Ha, J.; Cho, K.; Pak, J.; Seo, J.; Park, J.; Kim, J.-K.; Chung, S.; Hong, Y.; Lee, T. Transparent Large-Area MoS_2 Phototransistors with Inkjet-Printed Components on Flexible Platforms. *ACS Nano* **2017**, *11*, 10273.
(36) Kim, J.-K.; Song, Y.; Kim, T.-Y.; Cho, K.; Pak, J.; Choi, B. Y.; Shin, J.; Chung, S.; Lee, T. Analysis of Noise Generation and Electric Conduction at Grain Boundaries in CVD-Grown MoS_2 Field Effect Transistors. *Nanotechnology* **2017**, *28*, 47LT01.
(37) Lopez-Sanchez, O.; Lembke, D.; Kayci, M.; Radenovic, A.; Kis, A. Ultrasensitive Photodetectors Based on Monolayer MoS_2. *Nat. Nanotechnol.* **2013**, *8*, 497−501.
(38) Kufer, D.; Konstantatos, G. Highly Sensitive Encapsulated MoS_2 Photodetector with Gate Controllable Gain and Speed. *Nano Lett.* **2015**, *15*, 7307−7313.
(39) Zeng, L.; Tao, L.; Tang, C.; Zhou, B.; Long, H.; Chai, Y.; Lau, S. P.; Tsang, Y. H. High-Responsivity UV-Vis Photodetector Based on Transferable WS_2 Film Deposited by Magnetron Sputtering. *Sci. Rep.* **2016**, *6*, 20343.
(40) Kozawa, D.; Kumar, R.; Carvalho, A.; Amara, K. K.; Zhao, W.; Wang, S.; Toh, M.; Ribeiro, R. M.; Neto, A. H. C.; Matsuda, K.; Eda, G. Photocarrier Relaxation Pathway in Two-Dimensional Semiconducting Transition Metal Dichalcogenides. *Nat. Commun.* **2014**, *5*, 4543.
(41) Shi, H.; Yan, R.; Bertolazzi, S.; Brivio, J.; Gao, B.; Kis, A.; Jena, D.; Xing, H. G.; Huang, L. Exciton Dynamics in Suspended Monolayer and Few-Layer MoS_2 2D Crystals. *ACS Nano* **2013**, *7*, 1072−1080.
(42) Peelaers, H.; Van de Walle, C. G. Effects of Strain on Band Structure and Effective Masses in MoS_2. *Phys. Rev. B: Condens. Matter Mater. Phys.* **2012**, *86*, No. 241401R.
(43) Cheiwchanchamnangij, T.; Lambrecht, W. R. L. Quasiparticle Band Structure Calculation of Monolayer, Bilayer, and Bulk MoS_2. *Phys. Rev. B: Condens. Matter Mater. Phys.* **2012**, *85*, 205302.
(44) Chen, C.; Qiao, H.; Lin, S.; Luk, C. M.; Liu, Y.; Xu, Z.; Song, J.; Xue, Y.; Li, D.; Yuan, J.; Yu, W.; Pan, C.; Lau, S. P.; Bao, Q. Hghly Responsive MoS_2 Photodetectors Enhanced by Graphene Quantum Dots. *Sci. Rep.* **2015**, *5*, 11830.
(45) Wu, Y.-C.; Liu, C.-H.; Chen, S.-Y.; Shih, F.-Y.; Ho, P.-H.; Chen, C.-W.; Liang, C.-T.; Wang, W.-H. Extrinsic Origin of Persistent Photoconductivity in Monolayer MoS_2 Field Effect Transistors. *Sci. Rep.* **2015**, *5*, 11472.
(46) Miyamoto, Y.; Yoshikawa, D.; Takei, K.; Arie, T.; Akita, S. Effect of Buffer Layer on Photoresponse of MoS_2 Phototransistor. *Jpn. J. Appl. Phys.* **2018**, *57*, 06HB01.

DOI: 10.1021/acsnano.9b04829
ACS Nano 2019, 13, 9638−9646